JACS Au
AN OPEN ACCESS JOURNAL OF THE AMERICAN CHEMICAL SOCIETY

pubs.acs.org/jacsau
Article

Multimode Stimuli-Responsive Room-Temperature Phosphorescence Achieved by Doping Butterfly-like Fluorogens into Crystalline Small-Molecular Hosts

Zhaozhi Zhang, Qijing Wang, Xinyi Zhang, Ju Mei,* and He Tian

Cite This: JACS Au 2024, 4, 1954−1965

ABSTRACT: Materials with stimuli-responsive purely organic room-temperature phosphorescence (RTP) exempt from exquisite molecular design and complex preparation are highly desirable but still relatively rare. Moreover, most of them work in a single switching mode. Herein, we employ a versatile host−guest-doped strategy to facilely construct efficient RTP systems with multimode stimuli-responsiveness without ingenious molecular design. By conveniently doping butterfly-like guests, namely, *N*,*N*′-diphenyl-dihydrodibenzo[*a*,*c*]phenazines (DPACs), featured with vibration-induced emission into the small-molecular hosts via various methods, RTP systems with finely tunable photophysical properties are readily obtained. Through systematic mechanistic studies and with the aid of a series of control experiments, we unveil the critical role of the host crystallinity in achieving efficient RTP. By virtue of the inherent environmental sensitivity of both RTP and fluorescence of the DPACs, our systems exhibit multiple-stimuli-responsiveness with the luminescence not only switching between the fluorescence and phosphorescence but also continuously changing in the fluorescence color. Advanced dynamic anticounterfeiting and multilevel information encryption is thereby realized.

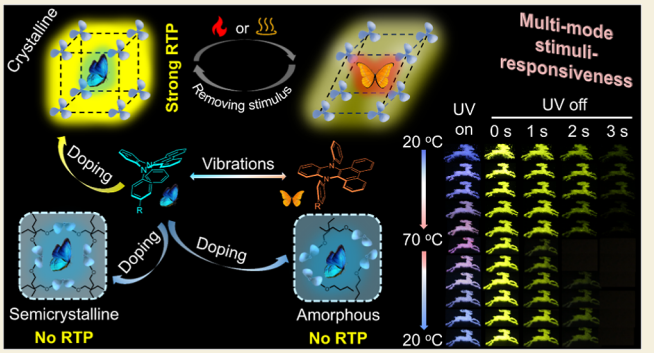

KEYWORDS: *room-temperature phosphorescence, vibration-induced emission, stimuli-responsiveness, crystallinity, N,N′-diphenyl-dihydrodibenzo[a,c]phenazines, anticounterfeiting and information encryption*

INTRODUCTION

Exploration of room-temperature phosphorescence (RTP) is a hot research topic in many fields such as materials science,[1−3] information security,[4−6] biochemistry,[7−9] and optoelectronics.[10,11] It is recognized that boosting the intersystem crossing (ISC) and reducing nonradiative transitions of the triplet excitons are two effective approaches to achieve phosphorescence.[12−15] Therefore, on the one hand, heteroatoms[16−18] such as nitrogen, oxygen, and sulfur or heavy atoms[19,20] such as bromine and iodine are often introduced to promote the $n-\pi^*$ transition, enhance the spin−orbit coupling (SOC), and promote the ISC. On the other hand, methods such as crystal engineering[21,22] and host−guest doping[23−25] are applied to use chemical or nonchemical bond interactions (such as hydrogen bond and van der Waals force) to stabilize the triplet state and reduce the nonradiative transitions. As a result, a large variety of room-temperature phosphorescence systems have been developed.[26−28]

Among all the RTP materials, the ones with stimulus-responsiveness are drawing increasing attention for their great application potential in the fields of sensing, information encryption, anticounterfeiting, data storage, and so on.[29−31] In comparison to the fluorescence-based stimulus-responsive materials which are susceptible to interference from background fluorescence, phosphorescence-based stimulus-responsive materials are more advantageous in longer lifetime and are more easily stimulated by the environment.[32−37] Despite this, most of the RTP-based stimulus-responsive materials depend on the monotonous interchange between the fluorescence intensity and phosphorescence intensity when a stimulus, such as heat, solvent fuming, light, etc., is applied. Moreover, the development of a considerable number of stimulus-responsive RTP materials usually requires cumbersome preparation processes and smart molecular design. However, to satisfy the requirements for practical applications such as advanced anticounterfeiting and information encryption, the stimulus-responsive RTP systems with multistate change achieved by

Received: February 28, 2024
Revised: April 26, 2024
Accepted: April 29, 2024
Published: May 9, 2024

https://doi.org/10.1021/jacsau.4c00187
JACS Au 2024, 4, 1954−1965

Scheme 1. Components, Fabrication, and the Working Mechanism of Our Proposed RTP Systems; (A) Molecular Structures of the Guests and Hosts; (B) Preparation Approaches to the Doped RTP Materials; (C) Diagram Illustration of the Stimuli-Responsiveness of the Doped RTP Materials

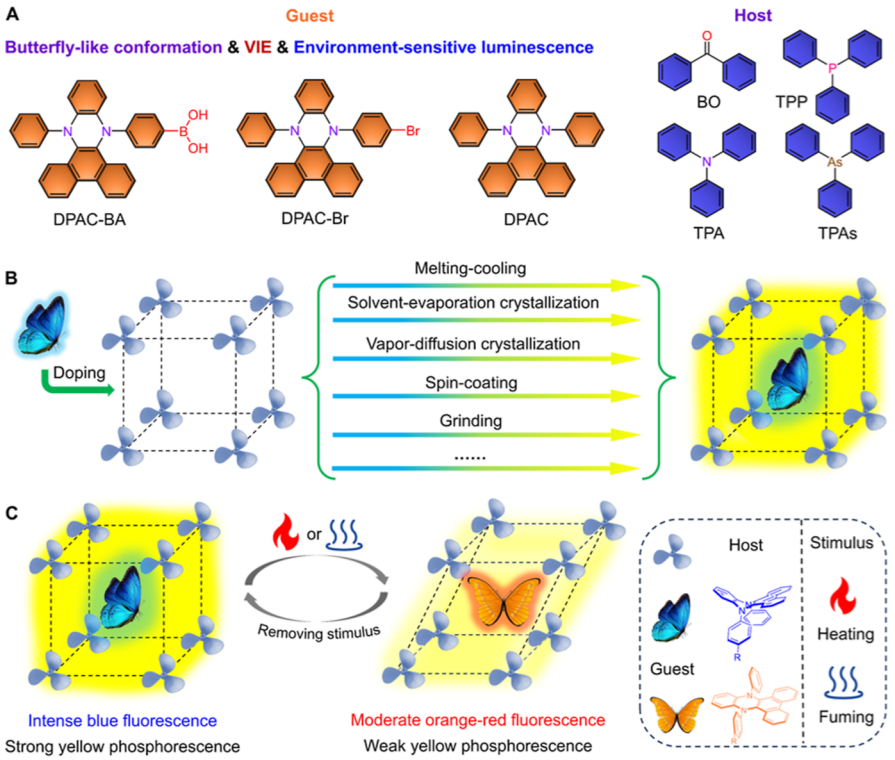

facile synthesis/fabrication without the need of complex molecular design are highly desirable.

In 2015, our group found that a class of phenazine derivatives exhibit unique photophysical phenomena. Specifically, DPACs display intrinsic blue emission stemmed from their saddle-shaped conformations in the confined state and abnormal orange-red fluorescence originated from the planar conformation in the unconfined state, with large Stokes shift of up to 200 nm.[38−45] It was later proven by a series of theoretical calculations and experiments that the orange-red emission is caused by the intramolecular bent-to-planar vibrations of the phenazine ring. Therefore, this phenomenon was named as vibration-induced emission (VIE).[38−45] Up until now, the DPAC derivatives have been widely explored for various purposes by virtue of their large Stokes shift and dual emissions.[46−66] For example, DAPC derivatives have been developed to probe physical parameters such as temperature,[50,51] viscosity,[52] and moisture,[53] to monitor physical processes such as self-assembly,[54] gelation,[55] and microphase separation[56] in real time, to detect chemical and biological species such as metal ions,[57,58] dicarboxylate dianions,[59,60] and glucose,[61] to detect and block influenza viruses,[62,63] to distinguish bacteria,[64] to conduct three-photon bioimaging,[65] and to construct mitochondria-specific photosensitizers.[66] To the best of our knowledge, the overwhelming majority of research studies related to VIE are based on the dual-fluorescence emission characteristics, but the phosphorescence properties of phenazine and its derivatives have received little attention.[67,68] Nevertheless, the *N*,*N*′-disubstituted-dihydrodibenzo[*a*,*c*]phenazine derivatives not only have the above-mentioned unique dual fluorescence emissions but also, what is even more important, that their fluorescence is easily affected by the surrounding environment, such as temperature, viscosity, etc., as a result of their flexible conformations. Therefore, it can be envisaged that the RTP materials based on phenazine derivatives might exhibit stimulus-responsiveness in both fluorescence and phosphorescence dimensions.

Here, as a proof of concept, we have successfully built a purely organic RTP system with multistimuli-responsiveness by the host−guest doping strategy which is widely recognized as a facile and universal approach to achieve RTP. The simplest and the most typical *N*,*N*′-diphenyl-dihydrodibenzo-[*a*,*c*]phenazine derivatives, namely, DPAC-BA, DPAC-Br, and DPAC, were chosen as the guests, the commonly used small molecules with low melting points, i.e., benzophenone (BO), triphenylamine (TPA), triphenylphosphine (TPP), and triphenylarsine (TPAs), were employed as the hosts (Scheme 1A). These RTP systems are readily accessible via different methods (Scheme 1B). In the meantime, we also carefully studied the RTP mechanism of our DPAC-based systems. It was found that the excited-state energy transfer (ET) between the host and guest molecules is the premise, and the good crystallinity of the hosts is also a requisite. This is the first time that the crucial role of the crystallinity of the host to the phosphorescence behaviors of the doped systems is clearly demonstrated. Moreover, both the fluorescence and phosphorescence of these phenazine derivatives is sensitive to the surrounding environment. In other words, these RTP materials would show response to any stimulus that would lead to the change in the host's crystalline framework and the conformation of the guest. To be more specific, the prepared doped RTP materials initially exhibit intense blue fluorescence and strong yellow phosphorescence, while the fluorescence gradually turns from blue to red passing through white light,

https://doi.org/10.1021/jacsau.4c00187
JACS Au 2024, 4, 1954−1965

and the phosphorescence is weakened gradually by heating or fuming. The fluorescence and phosphorescence could be restored after cooling or stopping fuming (Scheme 1C). Utilizing this multistimuli and multistate responsive feature, the doped RTP materials were applied to multilevel anticounterfeiting and advanced information encryption.

RESULTS AND DISCUSSION

Synthesis of Guest Molecules and Preparation of the Doped Materials

The borate-decorated *N*,*N*′-diphenyl-dihydrodibenzo[*a*,*c*]-phenazine DPAC-BA was first taken into consideration, as the borate is a Lewis acid which has been recognized to be conducive to the generation of phosphorescence. With the heavy atom, i.e., Br, which is supposed to boost the ISC, DPAC-Br was thus also included in the investigation. The unsubstituted *N*,*N*′-diphenyl-dihydrodibenzo[*a*,*c*]phenazine, namely, DPAC, which is the prototype VIE-active compound, was introduced for one thing as a control and for another as a model for the mechanistic study. In this way, a series of phenazine derivatives varying from DPAC-BA, DPAC-Br, to DPAC were selected as the guest compounds. DPAC was synthesized referring to the literature.[69] DPAC-Br was obtained by the Ullmann reaction, and DPAC-BA was acquired through the lithium halide exchange reaction of DPAC-Br (Scheme S1). The molecular structures of these compounds were fully characterized by ^{1}H NMR, ^{13}C NMR, and high-resolution mass spectrometry (HRMS) (Figures S1–S9). The host molecules were used directly as purchased without further treatment.

Measures that could afford the host–guest complexes are applicable to the achievement of doped RTP materials. It means that the doped materials could be prepared by diverse methods including melt-cooling, grinding, solvent–evaporation crystallization, vapor-diffusion crystallization, spin-coating, grinding, etc. Thermal analyses for the hosts and host–guest-doped materials were carried out (Figures S10, S11, and Table S1). The differential scanning calorimetry (DSC) curve shows that each of the host molecules has a low melting point, i.e., 50.1 °C for BO, 129.4 °C for TPA, 82.3 °C for TPP, and 63.0 °C for TPAs (Figure S10 and Table S1), which is conducive to the preparation of host–guest-doped materials through the melting-cooling method. The melting points of the doped materials are similar to those of the corresponding host, revealing that the guest molecules exert little impact on the thermal properties of the doped materials. According to the thermogravimetry analyses (TGA) curves (Figure S11 and Table S1), the host molecules have good thermal stability, which renders the prepared doped materials highly stable. We thus first attempted the melting-cooling method. Delightfully, all the host–guest-doped materials obtained via this method display a long afterglow at room temperature after the removal of radiation (Figure 1).

Considering the great impact of impurities on the phosphorescence,[70,71] we first examined the purity of the host molecules. As shown by the HPLC results, the commercially obtained BO, TPA, and TPAs have a purity exceeding 97%, while TPP possesses a relatively low purity of 95.3% (Figure S12). We then purified TPP by silica-gel column chromatography and recrystallization, acquiring a purity of 98.7%. When compared the materials obtained by doping DPAC-BA into the TPP before and after purification

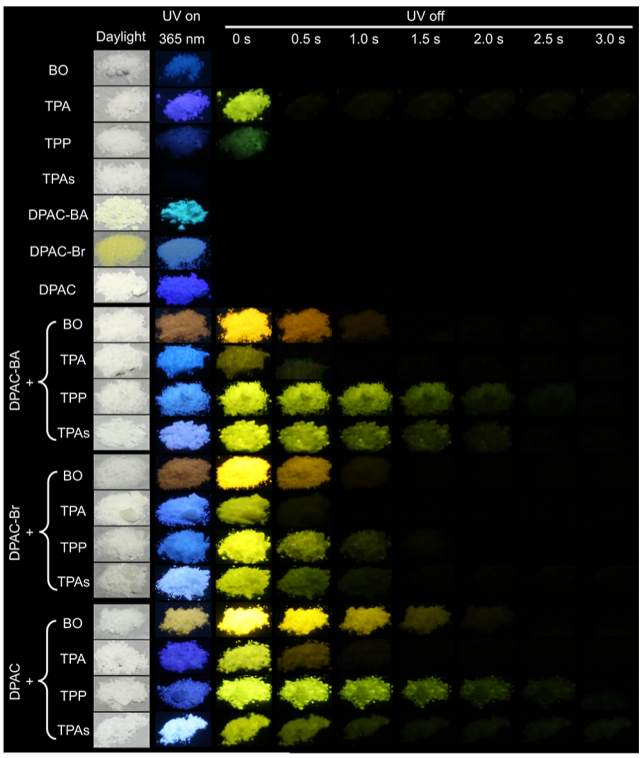

Figure 1. Long afterglow shown by the host–guest-doped materials. The daylight, fluorescence, and phosphorescence images of the hosts, guests, and host–guest-doped materials are displayed.

(Figure S13), there was no significant difference in both the fluorescence and phosphorescence. In view of the negligible impact of the host purity on the photophysical properties of the doped materials, the host molecules were directly used as purchased in the following experiments. To optimize the doping conditions, we explored the influence of the doping ratio on the RTP properties. When doping DPAC-BA into TPP at a doping ratio of 1:50–1:50,000, all the resulting doped materials show a long yellow afterglow with a phosphorescence lifetime of 90–408 ms (Figures S14 and S15). With the increase in the proportion of guests, the fluorescence of the doped materials is gradually intensified with an obvious red shift in the wavelength, while the phosphorescence first increases and then decreases, with the maximum at the doping ratio of 1:500 (Figure S15). Therefore, the guest-to-host molar ratio was set as 1:500 in the following experiments.

Photophysical Properties of the Doped Materials

The solid-state absorption maxima of the DPAC-BA-doped materials with BO, TPP, and TPAs as hosts are around 365 nm, similar to that of guest DPAC-BA (Figure S16). Differently, DPAC-BA + TPA shows a solid-state absorption of about 350 nm, which is consistent with that of TPA. The measurement of the excitation spectra of the doped materials in the solid state gave results similar to their solid-state absorption spectra (Figure S17A). BO displays multiple emissions in the phosphorescence spectra with a lifetime of 142 μs, while the DPAC-BA merely exhibits a fluorescence band with the maximum at about 480 nm (Figure S18A,B). We tested the photoluminescence (PL) spectra of BO at different temperatures (Figure S19A). As the temperature increases, the luminescence of BO gradually increases,

https://doi.org/10.1021/jacsau.4c00187
JACS Au 2024, 4, 1954–1965

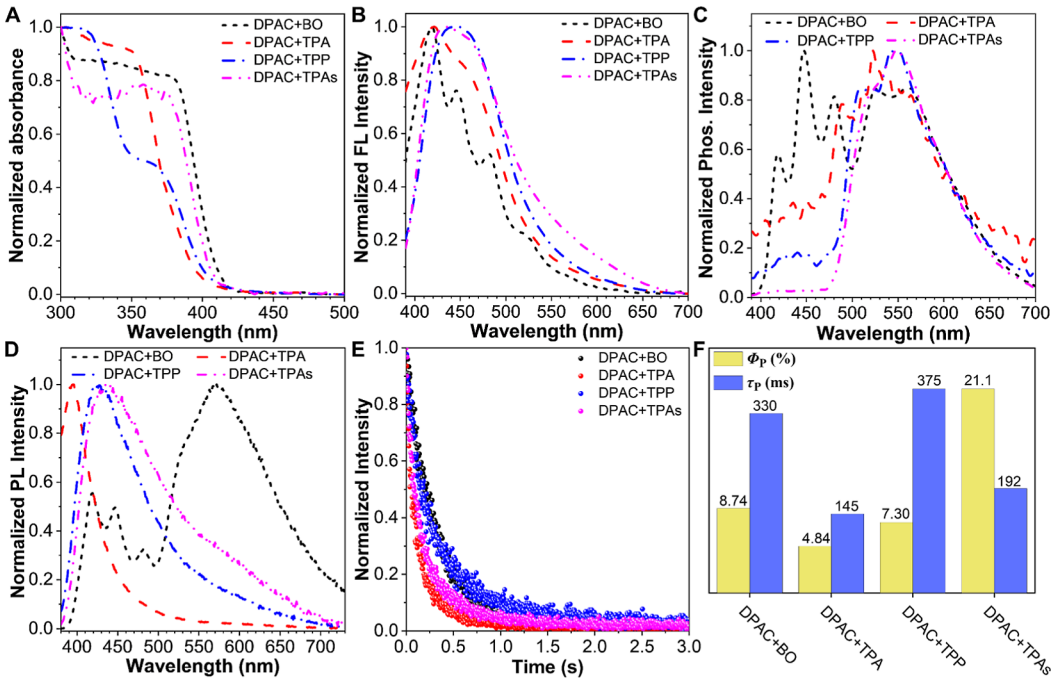

Figure 2. Photophysical properties of the doped RTP materials. The normalized (A) absorption, (B) fluorescence (FL) spectra, (C) phosphorescence (Phos.) spectra, (D) photoluminescence (PL) spectra, and (E) phosphorescence decay curves of DPAC + BO, DPAC + TPA, DPAC + TPP, and DPAC + TPAs, λ_{ex} = 365 nm, and delayed time = 0.1 ms. (F) Phosphorescence quantum yields and phosphorescence lifetimes of the doped RTP materials.

indicating the presence of thermally activated delayed fluorescence (TADF) rather than RTP. The fluorescence properties of DPAC-BA + BO are consistent with those of BO, while the phosphorescence emission peaks at 570 nm and is different from those of both the host and the guest. When DPAC-BA was doped into TPA, the fluorescence maximum of the resultant doped material was 450 nm, and the phosphorescence emission was very weak and centered at 530 nm, which is quite similar to that of TPA (Figure S18C,D). The fluorescence peak of DPAC-BA + TPP is at 430 nm, and its phosphorescence maximum is at 550 nm. In contrast, the phosphorescence of TPP is very weak and situated at 509 nm (Figure S18E,F). Unlike BO, TPP, and TPA, TPAs showed neither RTP nor TADF. However, DPAC-BA + TPAs display fluorescence emission at 437 nm, and phosphorescence emission peaked at 554 nm (Figure S18G,H). It could be seen that at the excitation of 365 nm (Figure S20A), the fluorescence emission maxima of DPAC-BA-doped materials are around 420−480 nm, and the phosphorescence emission maxima are around 530−570 nm (Figure S20B,C). DPAC-BA + TPA, DPAC-BA + TPP, and DPAC-BA + TPAs exhibit a single fluorescence emission peak in the photoluminescence spectra, while DPAC-BA + BO shows multiple emissions dominantly with phosphorescence emission (Figure S20D). The phosphorescence lifetimes of DPAC-BA-doped materials are in the range of 151−322 ms, and the phosphorescence quantum yields range from 5.10 to 15.1% (Figures S20E and S20F).

Despite the fact that the absorption maximum of DPAC-Br (at 410 nm) is quite distinct from that of DPAC-BA, the absorption and excitation spectra of the DPAC-Br-doped materials are fairly similar to those of the DPAC-BA-doped ones (Figures S17B and S21). Also different from DPAC-BA, DPAC-Br itself had phosphorescence emission peaked at 546 nm due to the heavy atom effect (Figure S22). When excited at 365 nm, the fluorescence spectrum of DPAC-Br + BO is similar to that of BO, but its phosphorescence spectrum peaked at 571 nm is different from those of both DPAC-Br and BO (Figure S22A,B). After DPAC-Br is doped into TPA, the fluorescence emission maximum of DPAC-Br + TPA is 423 nm and the phosphorescence peak is at 530 nm (Figure S22C,D). The DPAC-Br + TPP exhibits a fluorescence emission band at 442 nm and a phosphorescence emission peak at 556 nm (Figure S22E,F). The fluorescence and phosphorescence maximum of DPAC-Br + TPAs is at 457 and 554 nm, respectively (Figure S22G,H). Like the situation of DPAC-BA-doped materials, with the absorption maxima at 350−365 nm (Figure S23A), the fluorescence and phosphorescence maxima of the DPAC-Br-doped materials are also around 420−480 nm and 530−570 nm, respectively (Figure S23B,C). In the photoluminescence spectra, the fluorescence emission peaks of DPAC-Br + TPA, DPAC-Br + TPP, and DPAC-Br + TPAs are overwhelmingly higher than the phosphorescence bands, while DPAC-Br + BO exhibits multiple emissions with phosphorescence higher than the fluorescence (Figure S23D). The DPAC-Br-doped materials possess phosphorescence lifetime in the region of 111−236 ms and phosphorescence quantum yield varying from 9.20 to 12.8% (Figures S23E,F).

As exhibited in Figure 1, although without phosphorescence-promoting substituents, when DPAC was doped in the hosts, an obvious afterglow can still be clearly witnessed. Quite similar to the case of the DPAC-BA-doped materials, the solid-state absorption and excitation maxima of DPAC + BO, DPAC + TPP, and DPAC + TPAs are consistent with those of the guest molecule DPAC, while those of DPAC + TPA are at 350 nm (Figures 2A, S17C and S24). As displayed in Figure S25A,B, the fluorescence spectrum of DPAC + BO is

https://doi.org/10.1021/jacsau.4c00187
JACS Au 2024, 4, 1954−1965

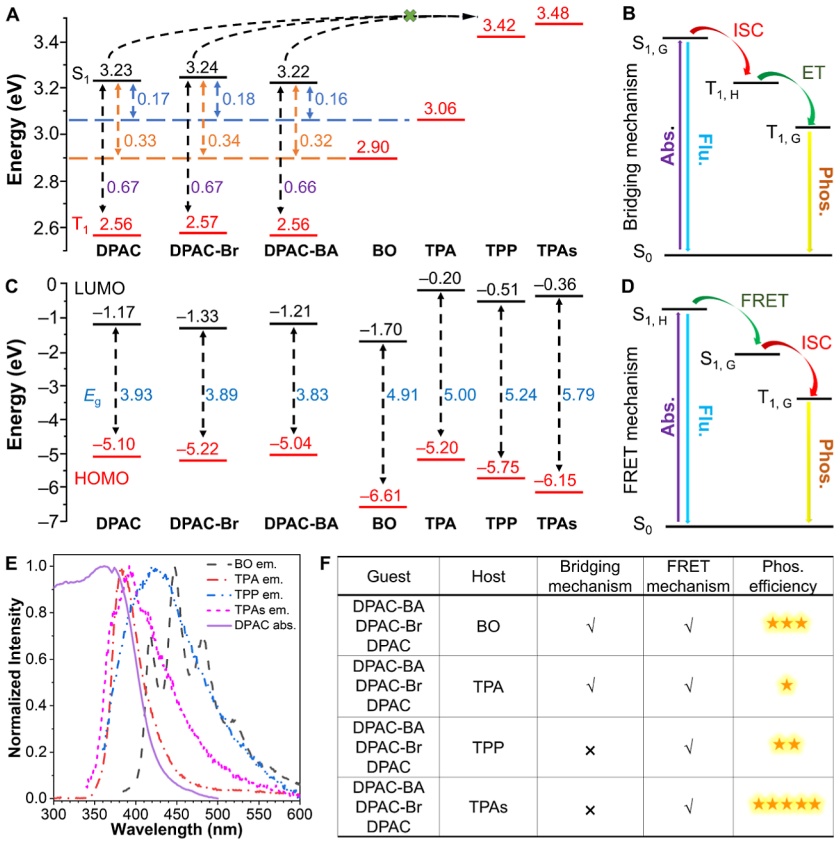

Guest	Host	Bridging mechanism	FRET mechanism	Phos. efficiency
DPAC-BA DPAC-Br DPAC	BO	√	√	★★★
DPAC-BA DPAC-Br DPAC	TPA	√	√	★
DPAC-BA DPAC-Br DPAC	TPP	×	√	★★
DPAC-BA DPAC-Br DPAC	TPAs	×	√	★★★★★

Figure 3. Theoretical calculation results of the doped materials. (A) Energy levels of guest and host molecules (red: T_1, black: S_1); (C) HOMO and LUMO of guest and host molecules (red: HOMO, black: LUMO); proposed mechanisms for RTP: (B) T_1 of the host molecules acts as a "bridge" between the S_1 and T_1 of the guest molecule; (D) there is a FRET from S_1 of the host to S_1 of the guest. (E) Normalized emission spectra of the hosts and the normalized absorbance spectrum of DPAC in the solid state. (F) Summary of the mechanism and the phosphorescence efficiency of each doped material.

consistent with that of BO, while the phosphorescence spectrum of DPAC + BO is composed of the TADF band of BO and a new phosphorescence emission band at 560 nm. DPAC displays emission bands in the phosphorescence spectrum. We tested the PL spectra of DPAC at different temperatures to confirm the nature of the emission (Figure S19B). The PL spectra of DPAC remain largely unchanged with temperature change. DPAC molecules have VIE properties, and as the temperature increases, the blue fluorescence should gradually decrease. This indicates the presence of TADF in DPAC, which leads to the increase of fluorescence with increasing temperature. Therefore, ultimately, the PL spectra of DPAC keep basically unchanged as temperature increases. Doping DPAC into TPA gives rise to a fluorescence emission at 421 nm and a very weak phosphorescence band at 530 nm (Figure S25C,D). The doped material DPAC + TPP shows a fluorescence emission peak at 448 nm and a phosphorescence emission band at 550 nm (Figure S25E,F). When DPAC is doped into TPAs, the case is quite similar to that of DPAC + TPP, with a fluorescence emission at 424 nm and the phosphorescence emission maximum at 553 nm (Figure S25G,H). The photoluminescence spectra of the DPAC-doped materials are in good consistency with the fluorescence and phosphorescence spectra, with the fluorescence maximum at around 420−480 nm and the phosphorescence maximum lying in the region of 530−560 nm (Figure 2B−D). As depicted in Figure 2E,F, the phosphorescence lifetimes of the DPAC-doped materials can be as long as 375 ms (DPAC + TPP), and the phosphorescence quantum yields can be as high as 21.1% (DPAC + TPAs). Obviously, as discussed above and shown in Table S2, different guest molecules behave similarly in the same host, indicating that the boric acid group and bromide atom are not the essential causes of the RTP of the doped materials. Noteworthily, DPAC without substituent shows the best RTP performance. On the other hand, when doped into different hosts, the same guest exhibits distinct photophysical properties. Generally speaking, guests perform best in TPP while worst in TPA, implying the critical role of host in the photophysical properties of the doped materials.

Mechanistic Studies on the RTP of the Doped Materials

The results of the photophysical investigation prompt us to conduct a detailed study on the RTP mechanism of our doped systems. We first tested the phosphorescence properties of these three guests at 77 K (Figure S26) and found that they all exhibit phosphorescence at 77 K with the maxima at about 550 nm. The phosphorescence bands are fairly similar to those of the doped materials at room temperature. Therefore, the phosphorescence of the doped materials is primarily originated from the guests.

To figure out why the RTP could be given out by the doped materials, we first conducted theoretical calculations. The S_1 energy level of the guest molecules is estimated to be 3.22−3.24 eV, and the T_1 energy level is calculated to be 2.56−2.57 eV, with their ΔE_{ST}s of 0.66−0.67 eV. The T_1 energy levels of

https://doi.org/10.1021/jacsau.4c00187
JACS Au 2024, 4, 1954−1965

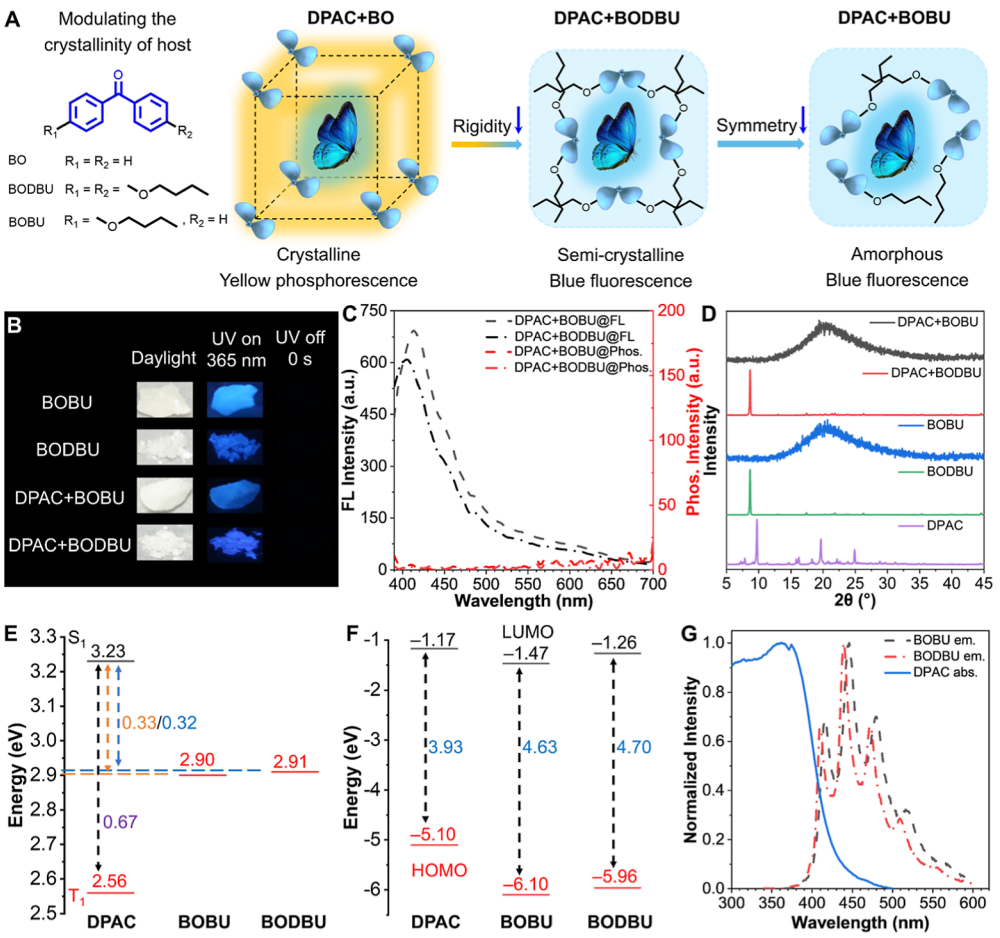

Figure 4. Mechanistic study results of the doped materials with control compounds. (A) Schematic illustration of the modulation of the molecular arrangements and crystallinity of the doped materials with different BO derivatives. (B) Daylight, fluorescence, and phosphorescence images of BOBU, BODBU, DPAC + BOBU, and DPAC + BODBU. (C) FL and Phos. spectra of DPAC + BOBU and DPAC + BODBU, λ_{ex} = 365 nm, delayed time = 0.1 ms. (D) XRD grams of DPAC, BOBU, BODBU, DPAC + BOBU, and DPAC + BODBU. (E) Energy levels of DPAC, BOBU, and BODBU (red: T_1, black: S_1). (F) HOMO and LUMO of DPAC, BOBU, and BODBU (red: HOMO, black: LUMO). (G) Normalized emission spectra of BOBU and BODBU and the normalized absorbance spectrum of DPAC.

BO and TPA are 2.90 and 3.06 eV, respectively, which are just in-between the S_1 and T_1 energy levels of the guest molecules (Figure 3A). The energy gaps between the T_1 of BO and S_1 of the guest molecules are about 0.32−0.34 eV, while those between the T_1 of TPA and S_1 of the guest molecules are in the region of 0.16−0.18 eV, respectively, which are smaller than the ΔE_{ST}s of the guest molecules. Therefore, the T_1 of BO and TPA could serve as a "bridge", rendering the electron transition from the S_1 state of the guest molecule to the T_1 state of the host molecule through ISC. The energy transfer from the T_1 state of the host molecule to the T_1 state of the guest molecule subsequently takes place, and then the triplet excitons finally relax to the ground state via radiative decay, giving out phosphorescence (Figure 3B). However, the T_1 energy levels of TPP and TPAs are 3.42 and 3.48 eV, which are higher than the S_1 energy levels of the guest molecules, indicating that the commonly used "bridge" mechanism is not applicable to our doping RTP systems with TPP and TPAs as hosts.

Hence, we further examine another possible mechanism that is also widely applied for the host−guest doping RTP systems (Figure 3C,D). As depicted in Figure 3C, the LUMO energy levels of the hosts are higher than those of the guests, while their HOMO energy levels are generally lower or similar to those of the guests, except BO. Moreover, the energy gaps (E_gs) of the guest molecules DPAC-BA (3.83 eV), DPAC-Br (3.89 eV), and DPAC (3.93 eV) are smaller than those of the host molecules (4.91, 5.00, 5.24, and 5.79 eV). It is recognized that the FRET process is prone to occur between the host and guest, and the RTP would be exhibited via the pathways, as shown in Figure 3D, when their HOMO, LUMO, and energy gaps meet the above conditions. The good overlaps between the emission of the host molecules and the absorbance of the guest molecules further confirm this possibility (Figures 3E and S27). Thus, it can be envisaged that in this case, the electrons first transition from the S_1 of the host molecule to the S_1 of the guest molecule through the FRET process, then to the T_1 of the guest molecule through ISC, and finally return to the ground state (S_0 of the guest molecule) in the form of radiative transitions to emit phosphorescence (Figure 3D). Combining the experimental and theoretical calculation results, it can be seen that although the RTP phosphorescence of all these host−guest doping materials can be interpreted with the mechanisms described in Figure 3B,D, the difference lying in the RTP performance can hardly be expressed with these mechanisms. For example, the systems with TPA as the host meet both the bridging mechanism and the FRET mechanism, and in theory, they should show the best RTP performance.

https://doi.org/10.1021/jacsau.4c00187
JACS Au 2024, 4, 1954−1965

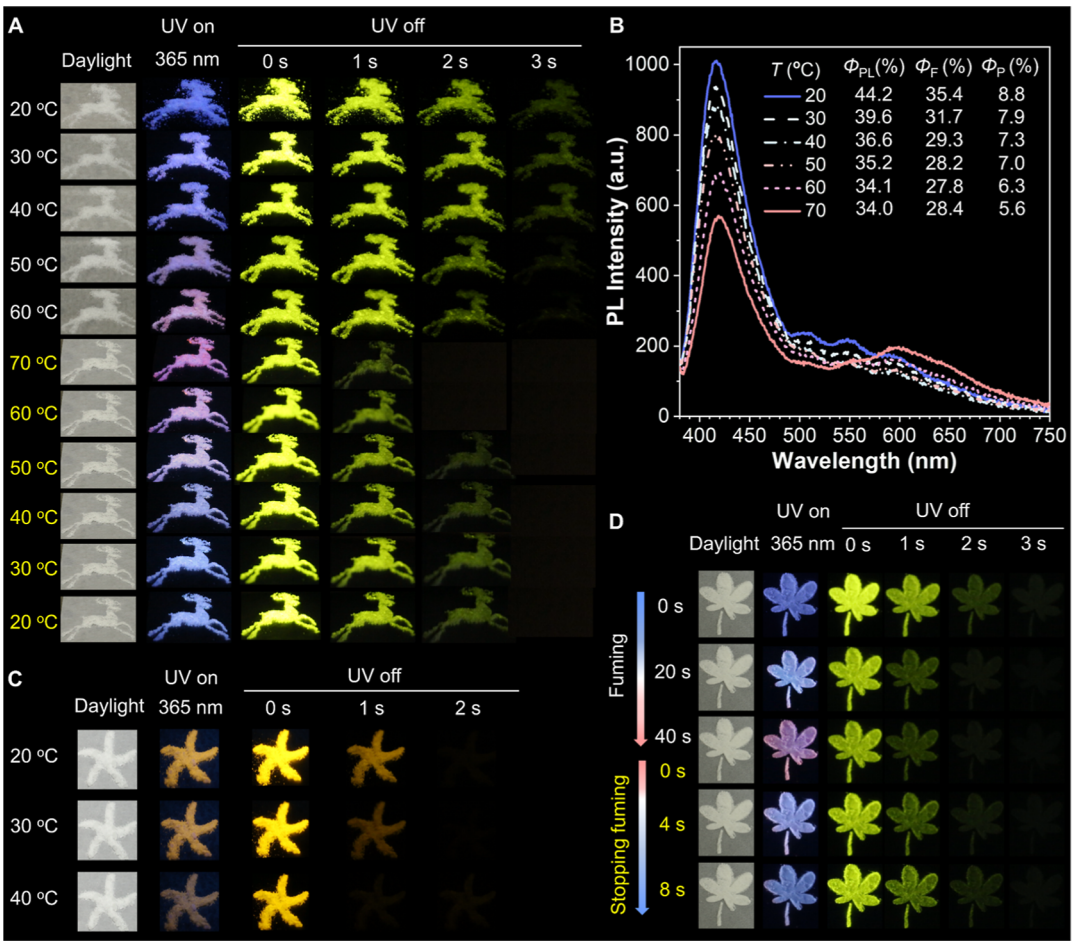

Figure 5. Stimuli-responsiveness of the doped RTP materials. (A) Temperature-responsiveness of the DPAC + TPP. (B) PL spectra, photoluminescence, fluorescence, and phosphorescence quantum yields of DPAC + TPP at different temperature. (C) Temperature-responsiveness of DPAC + BO. (D) Solvent-responsiveness of DPAC + TPP.

However, the experimental results are opposite to this (Figure 3F), which intrigued us to further determine what affects the RTP performance of our host−guest doping systems.

In view of the fact that crystallization usually promotes RTP emission, we first examine the crystallization properties of the hosts, guests, and doped materials. As revealed by the XRD results (Figure S28), all the doped materials are crystalline. However, the crystallinities of the ones with TPP as the host are the highest, while the ones with TPA as the host are relatively low, which are in good consistency with the RTP properties discussed above. In particular, the doped material DPAC + TPA showed the lowest crystallinity. Obviously, the RTP properties of the doped materials are closely associated with their crystallinity. Therefore, we modulated the crystallinity via the preparation processes. Take the doped material DPAC-BA + TPP, for example. When heating the mixture of DPAC-BA and TPP to melt, we adopted two different methods to cool it down to room temperature. The doped material obtained by liquid nitrogen quenching shows much shorter afterglow as compared to the one prepared via annealing (Figure S29). The XRD results also suggest that the annealed doped material has a higher crystallinity than that of the quenched one (Figure S30). As the XRD patterns of the doped materials more closely resemble those of their corresponding hosts (Figure S28), it can thus be inferred that the host crystallinity might exert an important effect on the RTP performance of the doped materials.

In order to further clarify the importance of the crystallinity of the hosts, we designed, synthesized, and characterized the derivatives of benzophenone, i.e., BOBU and BODBU (Scheme S2, and Figures S31−S36) and employed them as control hosts. As displayed in Figure 4, butoxy chain(s) was and were, respectively, introduced into the BO core to regulate the crystallinity and melting point of the host (Figure 4A). Both BOBU and BODBU are blue-fluorescent in the solid state. Similarly, the resultant doped materials DPAC + BOBU and DPAC + BODBU emit blue light under the irradiation of 365 nm UV light, with no obvious afterglow observed (Figure 4B), which agrees well with their fluorescence and phosphorescence spectra (Figure 4C). As expected, the XRD patterns proved that BOBU, BODBU, DPAC + BOBU, and DPAC + BODBU all hold low crystallinity (Figure 4D), which is in sharp contrast to the cases of BO and the doped materials with BO as a host. Therefore, the introduction of butoxy groups disorders the rigid and regular molecular arrangement of the host and subsequently decreases the crystallinity of the host and the resultant doped materials. Interestingly, the bis-butoxy-decorated BO shows higher crystallinity than the monobutoxy-substituted BO. It is probably due to the symmetrical molecular structure which enables the relatively ordered arrangement of BODBU molecules. Nevertheless, the loose

https://doi.org/10.1021/jacsau.4c00187
JACS Au 2024, 4, 1954−1965

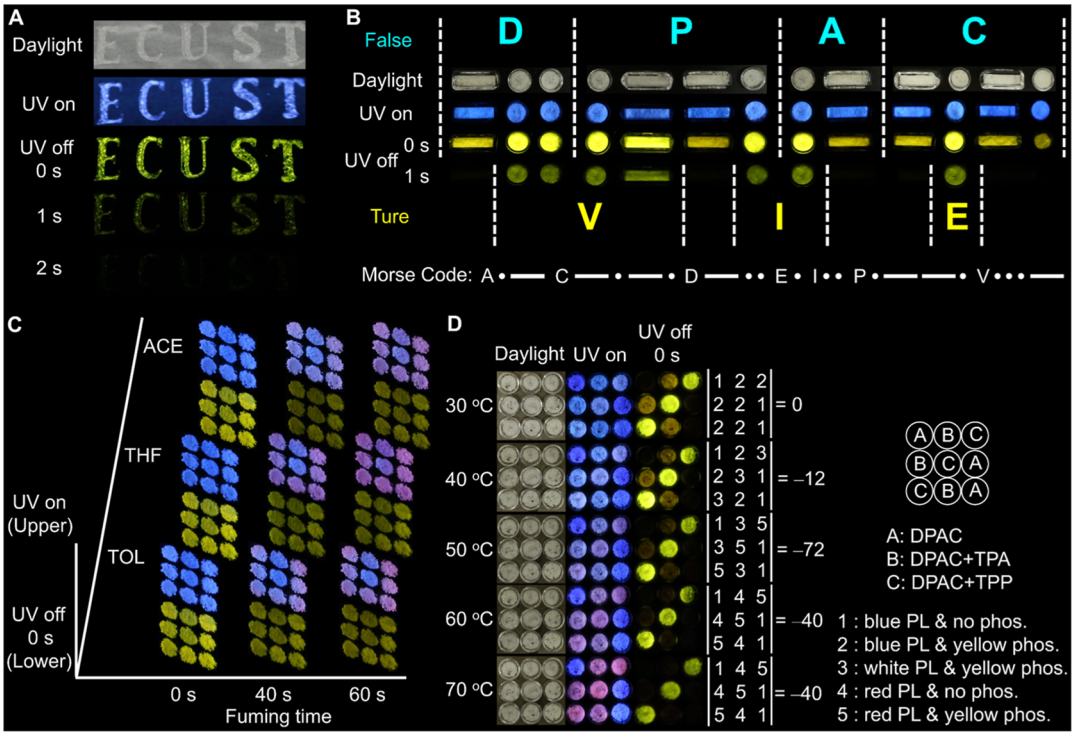

Figure 6. Anticounterfeiting and information encryption application of the doped RTP materials. (A) "ECUST" pattern observed under daylight, UV light, and after the removal of UV lamp, which was stamped on the filter paper with a seal using RTP-active DPAC + TPP as the printing mud. (B) Morse codes created with DPAC-BA + TPP and DPAC-BA + TPA, whose decryption is based on the difference between their afterglow time. (C) Time-dependent dynamic information encryption achieved by arranging DPAC-Br + TPA and DPAC-BA + TPA into a nine square grid and using different solvents to fumigate these doped materials. (D) Third-order determinants are composed of DPAC, DPAC + TPA, and DPAC + TPP, whose values are represented via their different responses to the change in temperature.

molecular packing and poor crystallization properties of BODBU still cannot impose sufficient restriction on the nonradiative decay of the triplet-state excitons (Figure 4A). It is noteworthy that the energy levels match both the "bridging" and FERT mechanisms mentioned above (Figure 4E–G), but they did not show an obvious room-temperature phosphorescence. Therefore, the crystallinity of the hosts indeed greatly affects the generation of RTP. Moreover, it can thus be concluded that under the premise of energy level matching, the higher the crystallinity, the better the RTP performance.

Applicability of the Doped RTP Materials

Stability and Accessibility of the Doped RTP Materials. To access the applicability of the doped RTP materials, we first examined their stability and found that DPAC + TPP still exhibits good RTP characteristics even after being stored under natural conditions for 8 months (Figure S37A). At the same time, even after being placed in water for 24 h, DPAC + TPP still displays high RTP performance (Figure S37B). It indicates that the good crystallization properties of the hosts can prevent water and oxygen from quenching phosphorescence, endowing the doped materials with high stability. Then, we tried to prepare doped materials by various other methods (Figures S37C and S38). Yellow-phosphorescent-doped materials could also be obtained by grinding, solvent–evaporation crystallization, vapor-diffusion crystallization, and spin-coating, suggesting that the DPAC-doped RTP materials are facilely accessible.

Stimuli-Responsiveness of the Doped RTP Materials. As the prototype VIE molecule, DPAC shows multiple fluorescence, which is easily and continuously changeable by the surrounding environment. Meanwhile, phosphorescence is also susceptible to an external environment. Therefore, the stimuli-responsiveness of the DPAC-doped RTP materials can be counted on (Figure 5). The fluorescence of the doped materials DPAC + TPP gradually changed from blue to red passing by the white-light region under the UV lamp, along with the temperature increase from 20 to 70 °C. Simultaneously, the phosphorescence intensity was gradually weakened, and the afterglow was shortened (Figure 5A). When the temperature decreased from 70 to 20 °C, the fluorescence and phosphorescence gradually returned to the original state. The fluorescence, phosphorescence, and overall photoluminescence all monotonously decrease with an increase in the temperature (Figure 5B). Nonetheless, at a temperature as high as 70 °C, the phosphorescence quantum yield of the doped material is still up to 5.6% (Figure 5B). We also studied the responsiveness of doped material DPAC + BO to temperature. As the temperature increased from 20 to 40 °C, the yellow photoluminescence was weakened, and so was the yellow phosphorescence. This is because the phosphorescence is stronger than the fluorescence in the doped material DPAC + BO (Figure 5C), which is quite different from the case of DPAC + TPP. We also applied the solvent as a stimulus. When fumed with THF, the fluorescence of DPAC + TPP gradually turned red, and the phosphorescence decreased. After stopping fuming, the fluorescence and phosphorescence of DPAC + TPP readily recovered to the state before fuming (Figure 5D).

Anticounterfeiting and Information Encryption Application of the Doped RTP Materials. It is clear that the DPAC derivative-doped materials show outstanding RTP properties and multimodal responsiveness to multiple stimuli.

https://doi.org/10.1021/jacsau.4c00187
JACS Au 2024, 4, 1954–1965

We hence explored the application potential of these doped RTP materials for anticounterfeiting and information encryption. First, we heated the doped material DPAC + TPP to melt and utilized this melt as printing mud, with which the "ECUST" pattern was stamped onto the filter paper using a seal. Under 365 nm UV light, the pattern exhibits intense blue fluorescence. After the removal of the UV irradiation, the real-time change of the pattern from blue fluorescence to yellow phosphorescence can be witnessed by naked eyes (Figure 6A). In such a simple way, dynamic anticounterfeiting is realized. Then, with the aid of DPAC-BA + TPP and DPAC-BA + TPA, advanced and dynamic information encryption is achieved in the mode of Morse code. Under daylight, UV light irradiation, or at the instant when the UV lamp is removed, the Morse code is in an encrypted state with the false output as "DPAC". While after removing the 365 nm irradiation for 1 s, since the afterglow of DPAC-BA + TPP is longer than that of DPAC-BA + TPA, the true information can be decrypted and output as "VIE" (Figure 6B).

Subsequently, we further took advantage of the solvent responsiveness of these doped materials to construct a time-dependent dynamic information encryption system. A nine-square grid was constructed by filling DPAC-BA + TPA and DPAC-Br + TPA into different cells. When fumed with different solvents (i.e., toluene, THF, acetone) for different times (0, 40, 60 s), the cells in the nine-square grid exhibit different emissions due to the differences in the crystallinity of these doped materials and the penetration ability of solvents. Upon fuming, the fluorescence of DPAC-BA + TPA turned red first, so the encrypted information, namely, the letter "U," was output by the difference in the fluorescence (Figure 6C). As the fuming time prolonged, the fluorescence of DPAC-Br + TPA also turned red, and then the decrypted information could be encrypted again. Moreover, we further explored the possibility of applying these doped materials for signal conversion. When DPAC, DPAC + TPA, and DPAC + TPP were put in different cells of a 3 × 3 grid, different luminescence signals could be delivered by different cells under different temperatures. When using different numbers to define different luminescence, namely, fluorescence and phosphorescence, a specific determinant can be built at a certain temperature. As a consequence, the luminescence or optical signals can be converted to digital information (Figure 6D). Notably, what we presented here are just examples; with these DPAC derivative-doped RTP materials, numerous and various anticounterfeiting, information encryption, and signal conversion models can be established for different purposes, demonstrating the high applicability of our RTP systems as advanced materials.

CONCLUSIONS

To sum up, we have facilely constructed a pure organic RTP system with multimodal multistimuli-responsiveness via simply doping VIE-active DPAC derivatives into small-molecular hosts. As a result, efficient RTP with a yellow afterglow, a long phosphorescence lifetime of up to 375 ms (DPAC + TPP), and a phosphorescence quantum yield as high as 21.1% (DPAC + TPAs) is achieved. These biocomponent RTP materials are highly stable and readily accessible via various very simple procedures, facilitating their applications in diverse fields. Thanks to the VIE and the RTP properties, both the fluorescence and phosphorescence can be finely and dynamically modulated by the environmental factors such as temperature and solvents, taking advantage of which dynamic anticounterfeiting, multilevel advanced information encryption, and convenient signal conversion are easily realized. What is also worth highlighting is that we clearly elaborate on the RTP mechanism of this system and the highly important role of the crystallinity of the hosts in the RTP performance of the doped materials. This work has not only established a versatile platform for the construction of high-performance stimuli-responsive RTP materials on the basis of DPAC derivatives but also provided good alternative materials for the applications such as anticounterfeiting and information encryption.

METHODS

Preparation of the Host–Guest-Doped Materials

Preparation via Melting-Cooling Method. The host and guest are mixed in a certain molar ratio first and then heated to molten to make the guest well-dispersed in the host framework. The mixture is finally cooled to room temperature to afford the host–guest-doped materials. The DPAC + TPP-doped materials are taken, for example. TPP (1.000 g, 3.813 mmol) and DPAC (3.31 mg, 0.007625 mmol) are mixed in a molar ratio of 500:1 in a Schlenk tube. The solid mixture is vacuumized and filled with N_2 for three times, and then heated to 85 °C under stirring for several minutes to yield a homogeneous molten. The host–guest-doped material DPAC + TPP is obtained when the mixture is cooled to room temperature.

Preparation via Solvent–Evaporation Crystallization. The host and guest are premixed in a certain molar ratio, and then good solvent is added to fully dissolve the host and the guest. The solvent is evaporated, giving the solids of the host–guest-doped material. The DPAC + TPP system is taken as an example. TPP (1.000 g, 3.813 mmol) and DPAC (3.31 mg, 0.007625 mmol) are mixed in a 500:1 molar ratio in a 50 mL single-necked flask. 10 mL of DCM is added into the flask. When TPP and DPAC are completely dissolved, DCM is evaporated by a rotatory evaporator, affording the doped material DPAC + TPP.

Preparation via Vapor-Diffusion Crystallization. To the premixed host and guest is added good solvent to make the host and guest completely dissolved. Then the solution is sealed and stored at room temperature to ensure slow evaporation of the solvent. Taking DPAC + TPP doped material, for instance, TPP (1.000 g, 3.813 mmol) and DPAC (3.31 mg, 0.007625 mmol) are mixed with a molar ratio of 500:1 in a 50 mL single-necked flask. To the flask, 10 mL of DCM is added to fully dissolve the mixture. The resulting solution is sealed in the flask with parafilm. DPAC + TPP is obtained upon the complete evaporation of DCM.

Preparation via Spin-Coating. Good solvent is added to the premixed host and guest first. When they are completely dissolved, the resulting solution is dropped onto a glass slide. The solvent is removed by the spin-coater to give the host–guest-doped materials. DPAC + TPP-doped material is taken as an example as well. The mixture of TPP (1.000 g, 3.813 mmol):DPAC (3.31 mg, 0.007625 mmol) = 500:1 (molar ratio) is placed in a 20 mL sample bottle. 5 mL of DCM is added to fully dissolve the mixture. The solution is dropped onto a glass slide and dried over a spin-coater, yielding the doped material DPAC + TPP.

Preparation via Grinding. The solids of the host and guest are mixed in a mortar first. A small amount of the good solvent is added afterward, and then the mixture is ground to give the doped material. Also, the doped material DPAC + TPP is taken, for example. TPP (1.000 g, 3.813 mmol) and DPAC (3.31 mg, 0.007625 mmol) are premixed with a molar ratio of 500:1 in a mortar and then 0.5 mL of DCM is added. The mixture is ground to fine powder, which is the doped material DPAC + TPP.

https://doi.org/10.1021/jacsau.4c00187
JACS Au 2024, 4, 1954–1965

■ ASSOCIATED CONTENT

Supporting Information

The Supporting Information is available free of charge at https://pubs.acs.org/doi/10.1021/jacsau.4c00187.

Full experimental procedures and original spectra of the characterization of compounds and additional figures in the photophysical property investigations and theoretical calculation (PDF)

■ AUTHOR INFORMATION

Corresponding Author

Ju Mei − *Key Laboratory for Advanced Materials, Feringa Nobel Prize Scientist Joint Research Center, Frontiers Science Center for Materiobiology and Dynamic Chemistry, Joint International Research Laboratory for Precision Chemistry and Molecular Engineering, Institute of Fine Chemicals, School of Chemistry and Molecular Engineering, East China University of Science & Technology, Shanghai 200237, China;* orcid.org/0000-0001-9992-8877; Email: daisymeiju@ecust.edu.cn

Authors

Zhaozhi Zhang − *Key Laboratory for Advanced Materials, Feringa Nobel Prize Scientist Joint Research Center, Frontiers Science Center for Materiobiology and Dynamic Chemistry, Joint International Research Laboratory for Precision Chemistry and Molecular Engineering, Institute of Fine Chemicals, School of Chemistry and Molecular Engineering, East China University of Science & Technology, Shanghai 200237, China*

Qijing Wang − *Key Laboratory for Advanced Materials, Feringa Nobel Prize Scientist Joint Research Center, Frontiers Science Center for Materiobiology and Dynamic Chemistry, Joint International Research Laboratory for Precision Chemistry and Molecular Engineering, Institute of Fine Chemicals, School of Chemistry and Molecular Engineering, East China University of Science & Technology, Shanghai 200237, China*

Xinyi Zhang − *Key Laboratory for Advanced Materials, Feringa Nobel Prize Scientist Joint Research Center, Frontiers Science Center for Materiobiology and Dynamic Chemistry, Joint International Research Laboratory for Precision Chemistry and Molecular Engineering, Institute of Fine Chemicals, School of Chemistry and Molecular Engineering, East China University of Science & Technology, Shanghai 200237, China*

He Tian − *Key Laboratory for Advanced Materials, Feringa Nobel Prize Scientist Joint Research Center, Frontiers Science Center for Materiobiology and Dynamic Chemistry, Joint International Research Laboratory for Precision Chemistry and Molecular Engineering, Institute of Fine Chemicals, School of Chemistry and Molecular Engineering, East China University of Science & Technology, Shanghai 200237, China;* orcid.org/0000-0003-3547-7485

Complete contact information is available at: https://pubs.acs.org/10.1021/jacsau.4c00187

Author Contributions

J. M. designed and supervised the project, analyzed the data, and revised and edited the manuscript. H. T. gave valuable suggestions and contributed to the manuscript revision. Z. Z. synthesized all the materials including the guest molecules and the control hosts, prepared all the doped materials, conducted all the photophysical measurements, and drafted the manuscript. Q. W. assisted in the compound synthesis and optical measurement. X. Z. performed the theoretical calculations. All authors have given approval to the final version of the manuscript.

Funding

This research was funded by the National Natural Science Foundation of China (21788102, 22275055, 21875064, and 21790361), the Shanghai Science and Technology Commission Basic Project Shanghai Natural Science Foundation (21ZR1417600), the Shanghai Municipal Science and Technology Major Project (2018SHZDZX03), the Programme of Introducing Talents of Discipline to Universities (B16017), the Shanghai Science and Technology Committee (17520750100), and the Fundamental Research Funds for the Central Universities.

Notes

The authors declare no competing financial interest.

■ ACKNOWLEDGMENTS

The authors thank the Research Center of Analysis and Test of East China University of Science and Technology for the help on the characterization.

■ REFERENCES

(1) Yan, X.; Peng, H.; Xiang, Y.; Wang, J.; Yu, L.; Tao, Y.; Li, H.; Huang, W.; Chen, R. Recent Advances on Host-Guest Material Systems toward Organic Room Temperature Phosphorescence. *Small* **2022**, *18*, 2104073.

(2) Yang, J.; Fang, M.; Li, Z. Stimulus-Responsive Room Temperature Phosphorescence Materials: Internal Mechanism, Design Strategy, and Potential Application. *Acc. Mater. Res.* **2021**, *2*, 644−654.

(3) Ma, L.; Liu, Y.; Tian, H.; Ma, X. Switching Singlet Exciton to Triplet for Efficient Pure Organic Room-Temperature Phosphorescence by Rational Molecular Design. *JACS Au* **2023**, *3*, 1835−1842.

(4) Lei, Y.; Dai, W.; Guan, J.; Guo, S.; Ren, F.; Zhou, Y.; Shi, J.; Tong, B.; Cai, Z.; Zheng, J.; Dong, Y. Wide-Range Color-Tunable Organic Phosphorescence Materials for Printable and Writable Security Inks. *Angew. Chem., Int. Ed.* **2020**, *59*, 16054−16060.

(5) Wu, H.; Wang, D.; Zhao, Z.; Wang, D.; Xiong, Y.; Tang, B. Z. Tailoring Noncovalent Interactions to Activate Persistent Room-Temperature Phosphorescence from Doped Polyacrylonitrile Films. *Adv. Funct. Mater.* **2021**, *31*, 2101656.

(6) Zheng, X.; Han, Q.; Lin, Q.; Li, C.; Jiang, J.; Guo, Q.; Ye, X.; Yuan, W. Z.; Liu, Y.; Tao, X. A Processable, Scalable, and Stable Full-Color Ultralong Afterglow System Based on Heteroatom-Free Hydrocarbon Doped Polymers. *Mater. Horiz.* **2023**, *10*, 197−208.

(7) Xiao, F.; Gao, H.; Lei, Y.; Dai, W.; Liu, M.; Zheng, X.; Cai, Z.; Huang, X.; Wu, H.; Ding, D. Guest-Host Doped Strategy for Constructing Ultralong-Lifetime Near-Infrared Organic Phosphorescence Materials for Bioimaging. *Nat. Commun.* **2022**, *13*, 186.

(8) Wang, Y.; Gao, H.; Yang, J.; Fang, M.; Ding, D.; Tang, B. Z.; Li, Z. High Performance of Simple Organic Phosphorescence Host-Guest Materials and Their Application in Time-Resolved Bioimaging. *Adv. Mater.* **2021**, *33*, 2007811.

(9) He, Z.; Gao, H.; Zhang, S.; Zheng, S.; Wang, Y.; Zhao, Z.; Ding, D.; Yang, B.; Zhang, Y.; Yuan, W. Z. Achieving Persistent, Efficient, and Robust Room-Temperature Phosphorescence from Pure Organics for Versatile Applications. *Adv. Mater.* **2019**, *31*, 1807222.

(10) Wang, T.; Su, X.; Zhang, X.; Nie, X.; Huang, L.; Zhang, X.; Sun, X.; Luo, Y.; Zhang, G. Aggregation-Induced Dual-Phosphorescence

from Organic Molecules for Nondoped Light-Emitting Diodes. *Adv. Mater.* **2019**, *31*, 1904273.
(11) Wu, M.; Li, J.; Huang, J.; Wang, X.; Wang, G.; Chen, X.; Li, X.; Chen, X.; Ding, S.; Zhang, H.; Zhang, K. The Unexpected Mechanism of Transformation from Conventional Room-Temperature Phosphorescence to TADF-Type Organic Afterglow Triggered by Simple Chemical Modification. *J. Mater. Chem. C* **2023**, *11*, 2291−2301.
(12) Guo, J.; Yang, C.; Zhao, Y. Long-Lived Organic Room-Temperature Phosphorescence from Amorphous Polymer Systems. *Acc. Chem. Res.* **2022**, *55*, 1160−1170.
(13) Bhattacharjee, I.; Hayashi, K.; Hirata, S. Key of Suppressed Triplet Nonradiative Transition-Dependent Chemical Backbone for Spatial Self-Tunable Afterglow. *JACS Au* **2021**, *1*, 945−954.
(14) Zhang, T.; Ma, X.; Wu, H.; Zhu, L.; Zhao, Y.; Tian, H. Molecular Engineering for Metal-Free Amorphous Materials with Room-Temperature Phosphorescence. *Angew. Chem., Int. Ed.* **2020**, *59*, 11206.
(15) Wang, Z.; Li, A.; Zhao, Z.; Zhu, T.; Zhang, Q.; Zhang, Y.; Tan, Y.; Yuan, W. Z. Accessing Excitation- and Time-Responsive Afterglows from Aqueous Processable Amorphous Polymer Films through Doping and Energy Transfer. *Adv. Mater.* **2022**, *34*, 2202182.
(16) Tian, Y.; Yang, J.; Liu, Z.; Gao, M.; Li, X.; Che, W.; Fang, M.; Li, Z. Multistage Stimulus-Responsive Room Temperature Phosphorescence Based on Host-Guest Doping Systems. *Angew. Chem., Int. Ed.* **2021**, *60*, 20259−20263.
(17) Wang, D.; Gong, J.; Xiong, Y.; Wu, H.; Zhao, Z.; Wang, D.; Tang, B. Z. Achieving Color-Tunable and Time-Dependent Organic Long Persistent Luminescence via Phosphorescence Energy Transfer for Advanced Anti-counterfeiting. *Adv. Funct. Mater.* **2023**, *33*, 2208895.
(18) Gao, M.; Tian, Y.; Li, X.; Gong, Y.; Fang, M.; Yang, J.; Li, Z. The Effect of Molecular Conformations and Simulated "Self-Doping" in Phenothiazine Derivatives on Room-Temperature Phosphorescence. *Angew. Chem., Int. Ed.* **2023**, *62*, No. e202214908.
(19) Dai, W.; Niu, X.; Wu, X.; Ren, Y.; Zhang, Y.; Li, G.; Su, H.; Lei, Y.; Xiao, J.; Shi, J.; Tong, B.; Cai, Z.; Dong, Y. Halogen Bonding: A New Platform for Achieving Multi-Stimuli-Responsive Persistent Phosphorescence. *Angew. Chem., Int. Ed.* **2022**, *61*, No. e202200236.
(20) Sun, S.; Ma, L.; Wang, J.; Ma, X.; Tian, H. Red-Light Excited Efficient Metal-Free Near-Infrared Room-Temperature Phosphorescent Films. *Natl. Sci. Rev.* **2022**, *9*, nwab085.
(21) Yu, J.; Ma, H.; Huang, W.; Liang, Z.; Zhou, K.; Lv, A.; Li, X.-G.; He, Z. Purely Organic Room-Temperature Phosphorescence Endowing Fast Intersystem Crossing from Through-Space Spin-Orbit Coupling. *JACS Au* **2021**, *1*, 1694−1699.
(22) Zhang, Q.-S.; Wang, S.-C.; Xiong, X.-H.; Fu, P.-Y.; Zhang, X.-D.; Fan, Y.-N.; Pan, M. High-Temperature and Dynamic RGB (Red-Green-Blue) Long-Persistent Luminescence in An Anti-Kasha Organic Compound. *Angew. Chem., Int. Ed.* **2022**, *61*, No. e202205556.
(23) Li, D.; Yang, Y.; Yang, J.; Fang, M.; Tang, B. Z.; Li, Z. Completely Aqueous Processable Stimulus Responsive Organic Room Temperature Phosphorescence Materials with Tunable Afterglow Color. *Nat. Commun.* **2022**, *13*, 347.
(24) Xie, Z.; Zhang, X.; Wang, H.; Huang, C.; Sun, H.; Dong, M.; Ji, L.; An, Z.; Yu, T.; Huang, W. Wide-Range Lifetime-Tunable and Responsive Ultralong Organic Phosphorescent Multi-Host/Guest System. *Nat. Commun.* **2021**, *12*, 3522.
(25) Wang, D.; Wu, H.; Gong, J.; Xiong, Y.; Wu, Q.; Zhao, Z.; Wang, L.; Wang, D.; Tang, B. Z. Unveiling the Crucial Contributions of Electrostatic and Dispersion Interactions to the Ultralong Room-Temperature Phosphorescence of H-Bond Crosslinked Poly(vinyl alcohol) Films. *Mater. Horiz.* **2022**, *9*, 1081−1088.
(26) Gong, Y.; Chen, G.; Peng, Q.; Yuan, W. Z.; Xie, Y.; Li, S.; Zhang, Y.; Tang, B. Z. Achieving Persistent Room Temperature Phosphorescence and Remarkable Mechanochromism from Pure Organic Luminogens. *Adv. Mater.* **2015**, *27*, 6195−6201.
(27) Wang, J.; Li, Q.; Zheng, J.; Yang, Y.; Liu, X.; Xu, B. N, B-Codoping Induces High-Efficiency Solid-State Fluorescence and Dual Emission of Yellow/Orange Carbon Dots. *ACS Sustainable Chem. Eng.* **2021**, *9*, 2224−2236.
(28) Gu, L.; Wu, H.; Ma, H.; Ye, W.; Jia, W.; Wang, H.; Chen, H.; Zhang, N.; Wang, D.; Qian, C.; An, Z.; Huang, W.; et al. Color-Tunable Ultralong Organic Room Temperature Phosphorescence from A Multicomponent Copolymer. *Nat. Commun.* **2020**, *11*, 944.
(29) Bi, X.; Shi, Y.; Peng, T.; Yue, S.; Wang, F.; Zheng, L.; Cao, Q. E. Multi-Stimuli Responsive and Multicolor Adjustable Pure Organic Room Temperature Fluorescence-Phosphorescent Dual-Emission Materials. *Adv. Funct. Mater.* **2021**, *31*, 2101312.
(30) Lu, L.; Wang, K.; Wu, H.; Qin, A.; Tang, B. Z. Simultaneously achieving high capacity storage and multilevel anti-counterfeiting using electrochromic and electrofluorochromic dual-functional AIE polymers. *Chem. Sci.* **2021**, *12*, 7058−7065.
(31) Ye, W.; Wang, Y.; Cao, T.; Meng, H.; Wang, C.; Hu, B.; Gao, Z.; Wang, C. Respiration-Responsive Colorful Room-Temperature Phosphorescent Materials and Assembly-Induced Phosphorescence Enhancement Strategies. *Small* **2023**, *19*, 2207403.
(32) Lei, Y.; Dai, W.; Li, G.; Zhang, Y.; Huang, X.; Cai, Z.; Dong, Y. Stimulus-Responsive Organic Phosphorescence Materials Based on Small Molecular Host-Guest Doped Systems. *J. Phys. Chem. Lett.* **2023**, *14*, 1794−1807.
(33) Yang, J.; Fang, M.; Li, Z. Stimulus-Responsive Room Temperature Phosphorescence in Purely Organic Luminogens. *InfoMat* **2020**, *2*, 791−806.
(34) Song, J.; Zhou, Y.; Pan, Z.; Hu, Y.; He, Z.; Tian, H.; Ma, X. An Elastic Organic Crystal with Multilevel Stimuli-Responsive Room Temperature Phosphorescence. *Matter* **2023**, *6*, 2005−2018.
(35) Li, D.; Yang, J.; Fang, M.; Tang, B. Z.; Li, Z. Stimulus-Responsive Room Temperature Phosphorescence Materials with Full-Color Tunability from Pure Organic Amorphous Polymers. *Sci. Adv.* **2022**, *8*, No. eabl8392.
(36) Song, J.; Ma, L.; Sun, S.; Tian, H.; Ma, X. Reversible Multilevel Stimuli-Responsiveness and Multicolor Room Temperature Phosphorescence Emission Based on A Single-Component System. *Angew. Chem., Int. Ed.* **2022**, *61*, No. e202206157.
(37) Dai, W.; Li, G.; Zhang, Y.; Ren, Y.; Lei, Y.; Shi, J.; Tong, B.; Cai, Z.; Dong, Y. Controllable Modulation of Efficient Phosphorescence through Dynamic Metal-Ligand Coordination for Reversible Anti-counterfeiting Printing of Thermal Development. *Adv. Funct. Mater.* **2023**, *33*, 2210102.
(38) Zhang, Z.; Wu, Y.-S.; Tang, K.-C.; Chen, C.-L.; Ho, J.-W.; Su, J.; Tian, H.; Chou, P.-T. Excited-State Conformational/Electronic Responses of Saddle-Shaped *N*, *N*′-Disubstituted-dihydrodibenzo[*a*, *c*]phenazines: Wide-Tuning Emission from Red to Deep Blue and White Light Combination. *J. Am. Chem. Soc.* **2015**, *137*, 8509−8520.
(39) Chen, W.; Chen, C.-L.; Zhang, Z.; Chen, Y.-A.; Chao, W.-C.; Su, J.; Tian, H.; Chou, P.-T. Snapshotting the Excited-State Planarization of Chemically Locked *N*, *N*′-Disubstituted-dihydrodibenzo[*a*, *c*]phenazines. *J. Am. Chem. Soc.* **2017**, *139*, 1636−1644.
(40) Zhang, Z.; Chen, C.-L.; Chen, Y.-A.; Wei, Y.-C.; Su, J.; Tian, H.; Chou, P.-T. Tuning the Conformation and Color of Conjugated Polyheterocyclic Skeletons by Installing *ortho*-Methyl Groups. *Angew. Chem., Int. Ed.* **2018**, *57*, 9880−9884.
(41) Zhang, Z.; Song, W.; Su, J.; Tian, H. Vibration-Induced Emission (VIE) of *N*, *N*′-Disubstituted-dihydrodibenzo[*a*, *c*]-phenazines: Fundamental Understanding and Emerging Applications. *Adv. Funct. Mater.* **2019**, *30*, 1902803.
(42) Sun, G.; Wei, Y.; Zhang, Z.; Lin, J.; Liu, Z.; Chen, W.; Su, J.; Chou, P.-T.; Tian, H. Diversified Excited-State Relaxation Pathways of Donor-Linker-Acceptor Dyads Controlled by A Bent-to-Planar Motion of the Donor. *Angew. Chem., Int. Ed.* **2020**, *59*, 18611−18618.
(43) Zhang, Z.; Sun, G.; Chen, W.; Su, J.; Tian, H. The Endeavor of Vibration-Induced Emission (VIE) for Dynamic Emissions. *Chem. Sci.* **2020**, *11*, 7525−7537.
(44) Jin, X.; Li, S.; Guo, L.; Hua, J.; Qu, D.-H.; Su, J.; Zhang, Z.; Tian, H. Interplay of Steric Effects and Aromaticity Reversals to

https://doi.org/10.1021/jacsau.4c00187
JACS Au 2024, 4, 1954−1965

Expand the Structural/Electronic Responses of Dihydrophenazines. *J. Am. Chem. Soc.* **2022**, *144*, 4883−4896.
(45) Jin, X.; Guo, S.; Wang, X.; Cong, M.; Chen, J.; Zhang, Z.; Su, J.; Qu, D.-H.; Tian, H. Sequential Multistep Excited-State Structural Transformations in *N,N′*-Disubstituted-dihydrodibenzo[*a*, *c*]-phenazine Ffluorophores. *Angew. Chem., Int. Ed.* **2023**, *62*, No. e202305572.
(46) Yang, S.; Zhao, C.-X.; Crespi, S.; Li, X.; Zhang, Q.; Zhang, Z.; Mei, J.; Tian, H.; Qu, D.-H. Reversibly Modulating A Conformation-Adaptive Fluorophore in [2]Catenane. *Chem* **2021**, *7*, 1544−1556.
(47) Zong, Z.; Zhang, Q.; Qiu, S.-H.; Wang, Q.; Zhao, C.; Zhao, C.-X.; Tian, H.; Qu, D.-H. Dynamic Timing Control over Multicolor Molecular Emission by Temporal Chemical Locking. *Angew. Chem., Int. Ed.* **2022**, *61*, No. e202116414.
(48) Gu, F.; Li, Y.; Jiang, T.; Su, J.; Ma, X. Polymer-Stretching Photoluminescent Regulation by Doping A Single Fluorescent Molecule. *CCS Chem.* **2022**, *3*, 3014.
(49) Zou, Q.; Chen, X.; Zhou, Y.; Jin, X.; Zhang, Z.; Qiu, J.; Wang, R.; Hong, W.; Su, J.; Qu, D.-H.; Tian, H. Photoconductance from the Bent-to-Planar Photocycle between Ground and Excited States in Single-Molecule Junctions. *J. Am. Chem. Soc.* **2022**, *144*, 10042−10052.
(50) Liu, H.; Song, W.; Chen, X.; Mei, J.; Zhang, Z.; Su, J. Temperature-Responsive Molecular Liquids Based on Dihydrophenazines for Dynamic Multicolor-Fluorescent Anti-counterfeiting and Encryption. *Mater. Chem. Front.* **2021**, *5*, 2294−2302.
(51) Song, W.; Ye, W.; Shi, L.; Huang, J.; Zhang, Z.; Mei, J.; Su, J.; Tian, H. Smart Molecular Butterfly: An Ultra-Sensitive and Range-Tunable Ratiometric Thermometer Based on Dihydrophenazines. *Mater. Horiz.* **2020**, *7*, 615−623.
(52) Wang, H.; Li, Y.; Zhang, Y.; Mei, J.; Su, J. A New Strategy for Achieving Single-Molecular White-Light Emission: Using Vibration-Induced Emission (VIE) plus Aggregation-Induced Emission (AIE) Mechanisms as A Two-Pronged Approach. *Chem. Commun.* **2019**, *55*, 1879−1882.
(53) Sun, G.; Pan, J.; Wu, Y.; Liu, Y.; Chen, W.; Zhang, Z.; Su, J. Supramolecular Assembly-Driven Color-Tuning and White-Light Emission Based on Crown-Ether-Functionalized Dihydrophenazine. *ACS Appl. Mater. Interfaces* **2020**, *12*, 10875−10882.
(54) Huang, Z.; Jiang, T.; Wang, J.; Ma, X.; Tian, H. Real-Time Visual Monitoring of Kinetically Controlled Self-Assembly. *Angew. Chem., Int. Ed.* **2021**, *60*, 2855−2860.
(55) Sun, G.; Zhou, H.; Liu, Y.; Li, Y.; Zhang, Z.; Mei, J.; Su, J. Ratiometric Indicator Based on Vibration-Induced Emission for in situ and Real-Time Monitoring of Gelation Processes. *ACS Appl. Mater. Interfaces* **2018**, *10*, 20205−20212.
(56) Zhang, Y.; Li, Y.; Wang, H.; Zhang, Z.; Feng, Y.; Tian, Q.; Li, N.; Mei, J.; Su, J.; Tian, H. Measuring the Microphase Separation Scale of Polyurethanes with A Vibration-Induced Emission-Based Ratiometric "Fluorescent Ruler. *ACS Appl. Mater. Interfaces* **2019**, *11*, 39351−39358.
(57) Zhou, H.; Mei, J.; Chen, Y.-A.; Chen, C.-L.; Chen, W.; Zhang, Z.; Su, J.; Chou, P.-T.; Tian, H. Phenazine-Based Ratiometric Hg^{2+} Probes with Well-Resolved Dual Emissions: A New Sensing Mechanism by Vibration-Induced Emission (VIE). *Small* **2016**, *12*, 6542−6546.
(58) Li, Y.; Liu, Y.; Zhou, H.; Chen, W.; Mei, J.; Su, J. Ratiometric Hg^{2+}/Ag^{+} Probes with Orange Red-White-Blue Fluorescence Response Constructed by Integrating Vibration-Induced Emission with An Aggregation-Induced Emission Motif. *Chem.—Eur. J.* **2017**, *23*, 9280−9287.
(59) Zhou, Z.; Chen, D.-G.; Saha, M. L.; Wang, H.; Li, X.; Chou, P.-T.; Stang, P. J. Designed Conformation and Fluorescence Properties of Self-Assembled Phenazine-Cored Platinum(II) Metallacycles. *J. Am. Chem. Soc.* **2019**, *141*, 5535−5543.
(60) Chen, W.; Guo, C.; He, Q.; Chi, X.; Lynch, V. M.; Zhang, Z.; Su, J.; Tian, H.; Sessler, J. L. Molecular Cursor Caliper: A Fluorescent Sensor for Dicarboxylate Dianions. *J. Am. Chem. Soc.* **2019**, *141*, 14798−14806.
(61) Ramos-Soriano, J.; Benitez-Benitez, S. J.; Davis, A. P.; Galan, M. C. A Vibration-Induced Emission-Based Fluorescent Chemosensor for the Selective and Visual Recognition of Glucose. *Angew. Chem., Int. Ed.* **2021**, *60*, 16880−16884.
(62) Dou, W.-T.; Qin, Z.-Y.; Li, J.; Zhou, D.-M.; He, X.-P. Self-Assembled Sialyllactosyl Probes with Aggregation-Enhanced Properties for Ratiometric Detection and Blocking of Influenza Viruses. *Sci. Bull.* **2019**, *64*, 1902−1909.
(63) Dou, W.-T.; Wang, X.; Liu, T.; Zhao, S.; Liu, J.-J.; Yan, Y.; Li, J.; Zhang, C.-Y.; Sedgwick, A. C.; Tian, H.; Sessler, J. L.; Zhou, D.-M.; He, X.-P. A Homogeneous High-Throughput Array for the Detection and Discrimination of Influenza A Viruses. *Chem* **2022**, *8*, 1750−1761.
(64) Hu, X.-L.; Gan, H.-Q.; Qin, Z.-Y.; Liu, Q.; Li, M.; Chen, D.; Sessler, J. L.; Tian, H.; He, X.-P. Phenotyping of Methicillin-Resistant Staphylococcus Aureus Using a Ratiometric Sensor Array. *J. Am. Chem. Soc.* **2023**, *145*, 8917−8926.
(65) Li, S.; He, M.; Jin, X.; Geng, W.; Li, C.; Li, X.; Zhang, Z.; Qian, J.; Hua, J. Extending the Stokes Shifts of Donor-Acceptor Fluorophores by Regulating the Donor Configuration for in vivo Three-Photon Fluorescence Imaging. *Chem. Mater.* **2022**, *34*, 5999−6008.
(66) Zhang, Z.; Wang, Q.; Zhang, X.; Mei, D.; Mei, J. Modulating the Luminescence, Photosensitizing Properties, and Mitochondria-Targeting Ability of D-π-A-Structured Dihydrodibenzo[*a*, *c*]-phenazines. *Molecules* **2023**, *28*, 6392.
(67) Gu, F.; Jiang, T.; Ma, X. Visually Monitoring the Compactness of Polymer Matrixes Coded by Disparate Luminescence. *ACS Appl. Mater. Interfaces* **2021**, *13*, 43473−43479.
(68) Su, Y.; Jin, X.; Su, J.; Feng, Y.; Wang, Q.; Zhang, Z.; Tian, H.; Ma, X. Radical Afterglow Emission Harnessed by Doping *N*, *N′*-Diaryl-5,10-dihydrophenazines to Epoxy Resins. *Adv. Opt. Mater.* **2023**, *11*, 2300604.
(69) Wang, H.; Zhang, Z.; Zhou, H.; Wang, T.; Su, J.; Tong, X.; Tian, H. Cu-Catalyzed C-H Amination/Ullmann N-Arylation Domino Reaction: A Straightforward Synthesis of 9,14-Diaryl-9,14-dihydrodibenzo[*a*, *c*]phenazine. *Chem. Commun.* **2016**, *52*, 5459−5462.
(70) Chen, C.; Chi, Z.; Chong, K. C.; Batsanov, A. S.; Yang, Z.; Mao, Z.; Yang, Z.; Liu, B. Carbazole Isomers Induce Ultralong Organic Phosphorescence. *Nat. Mater.* **2021**, *20*, 175−180.
(71) Ding, B.; Ma, L.; Huang, Z.; Ma, X.; Tian, H. Engendering Persistent Organic Room Temperature Phosphorescence by Trace Ingredient Incorporation. *Sci. Adv.* **2021**, *7*, No. eabf9668.

https://doi.org/10.1021/jacsau.4c00187
JACS Au 2024, 4, 1954−1965